

A framework for estimating potential fluid flow from digital imagery

Aaron Luttmann,^{1,a)} Erik M. Bollt,^{1,b)} Ranil Basnayake,^{1,c)} Sean Kramer,^{1,d)}
 and Nicholas B. Tuffillaro^{2,e)}

¹Department of Mathematics, Clarkson University, P.O. Box 5815, Potsdam, New York 13699-5815, USA

²College of Earth, Oceanic, and Atmospheric Sciences, Oregon State University, 104 CEOAS Administration Building, Corvallis, Oregon 97331-5503, USA

(Received 30 April 2012; accepted 29 August 2013; published online 11 September 2013)

Given image data of a fluid flow, the flow field, $\langle u, v \rangle$, governing the evolution of the system can be estimated using a variational approach to optical flow. Assuming that the flow field governing the advection is the symplectic gradient of a stream function or the gradient of a potential function—both falling under the category of a *potential flow*—it is natural to re-frame the optical flow problem to reconstruct the stream or potential function directly rather than the components of the flow individually. There are several advantages to this framework. Minimizing a functional based on the stream or potential function rather than based on the components of the flow will ensure that the computed flow is a potential flow. Next, this approach allows a more natural method for imposing scientific priors on the computed flow, via regularization of the optical flow functional. Also, this paradigm shift gives a framework—rather than an algorithm—and can be applied to nearly any existing variational optical flow technique. In this work, we develop the mathematical formulation of the potential optical flow framework and demonstrate the technique on synthetic flows that represent important dynamics for mass transport in fluid flows, as well as a flow generated by a satellite data-verified ocean model of temperature transport. © 2013 AIP Publishing LLC. [<http://dx.doi.org/10.1063/1.4821188>]

We present a method for constructing the velocity field of a fluid flow from image intensity data. Given that the flow field is the gradient of a potential function, the potential can be reconstructed directly, rather than the constructing the components of the flow individually. This allows an alternative viewpoint of regularizing optical flow and leads to improved reconstructions, which we demonstrate on synthetic and data-verified flow structures relevant to mass transport in fluids.

I. INTRODUCTION

Optical flow is the term used to describe the computation of a vector field describing the apparent motion between time-adjacent images of the same scene. Since Horn and Schunck¹ introduced their seminal algorithm, there has been a substantial literature presenting a variety of approaches to optical flow, and there is also an extensive literature comparing and contrasting these methods with respect to their computational complexities and abilities to accurately capture the underlying flow fields (for example, Refs. 2–9).

In the last decade, optical flow algorithms have been adapted for analyzing fluid flows in connection with and in comparison to particle image velocimetry (PIV),^{10,11} geophysical fluid flows,^{12,13} atmospheric motion,² and laboratory

experimental fluid flows,¹⁴ and an extensive survey of the fluids literature on optical flow is given in Ref. 15. Whereas some image-based techniques for fluid dynamics analysis require rigid experimental conditions—such as PIV—optical flow based techniques can be used in more general settings, and that is one of the primary reasons for developing optical flow-based approaches to fluid dynamics analysis. For example, given satellite data, it could be possible to analyze the dynamics of species transport in the ocean¹⁶ or other kinds of pseudo-transport;¹⁷ analysis that could not be done from methods like PIV. The primary challenge in determining whether optical flow is appropriate to use in a given application is understanding how the 2D image projections of the flow relate to the physical 3D flow, which heavily depends on the application being studied.

Given time-varying image data, $I(x, y, t)$, on a spatial domain $\Omega \subset \mathbb{R}^2$ and a temporal domain $[0, T]$, Horn and Schunck¹ modeled the evolution of the image intensities as an advection governed by

$$I_t(x, y, t) = -\nabla I(x, y, t) \cdot \langle u(x, y, t), v(x, y, t) \rangle, \quad (1)$$

where u and v are the horizontal and vertical components of the flow field. This model is derived from a local conservation of intensity and assuming that each of the components of the flow field is smooth. The flow is computed as a minimizer of

$$E_\alpha(u, v) = \int_\Omega (I_t + I_x u + I_y v)^2 d\Omega + \alpha R(u, v), \quad (2)$$

where $R(u, v) = \int_\Omega u_x^2 + u_y^2 + v_x^2 + v_y^2 d\Omega$ was their chosen regularization and $\alpha > 0$ is a regularization parameter that

^{a)}Electronic mail: aluttmann21@gmail.com.

^{b)}Electronic mail: bolltem@clarkson.edu.

^{c)}Electronic mail: basnayrk@clarkson.edu.

^{d)}Electronic mail: skramer@norwich.edu.

^{e)}Electronic mail: nbt.osu@gmail.com.

serves as a weighting factor between the least squares data fidelity and the regularization.

This formulation is appropriate for computing “flow” fields associated with rigid-body motions of non-reflectant surfaces, but different physical models can also be incorporated into the data fidelity to use such an approach for computing fluid flows. Rather than assuming a system evolves according to Eq. (1), Corpetti *et al.* proposed in Refs. 18–22 to model a fluid system as evolving according to the continuity equation,

$$I_t(x, y, t) = -\text{div}(I(x, y, t)\langle u(x, y, t), v(x, y, t) \rangle), \quad (3)$$

resulting in an optical flow energy of the form

$$E_\alpha(u, v) = \int_{\Omega} (I_t + \text{div}(I\langle u, v \rangle))^2 d\Omega + \alpha R(u, v), \quad (4)$$

where $R(u, v)$ is an appropriate regularization scheme and u and v depend on x, y , and t (which we drop from the notation from here on). They proposed to regularize using the “second-order div-curl regularization” of Ref. 23, which is given by

$$R(u, v) = \int_{\Omega} \|\nabla \text{div}(\langle u, v \rangle)\|^2 + \|\nabla \text{curl}(\langle u, v \rangle)\|^2 d\Omega. \quad (5)$$

Their work served as motivation for Kohlberger *et al.*²⁴ to reformulate the optical flow problem, using the same regularization, in order to reconstruct the components of the Helmholtz decomposition of the flow, allowing to capture the curl-free and divergence-free components (though not the laminar component). This was a departure from classical optical flow, where the flow components are computed along the horizontal and vertical axes.

The approach presented here is largely motivated by that work and also shifts from reconstructing the horizontal and vertical components of the flow and focuses on flows that can be represented as the gradient of a potential function or as the symplectic gradient of a stream function. Whereas large-scale fluid flows, such as oceanic flows, are almost never globally representable by a single potential function, many local dynamical structures of interest, such as vortices and outflows (sources), can be modeled in this way, and we demonstrate that our method captures these local structures quite well. This is a simpler model than that used in Ref. 24, but it presents several advantages. First, our methods are simpler to implement computationally, as it requires solving one minimization problem rather than two coupled problems. More importantly, the approach described in the sequel allows to impose scientific priors, via regularization, directly on the potential rather than on the separate div-free and curl-free or u - v components of the flow.

When combined with different regularization schemes, the two system evolution models, (1) and (3), lead to a collection of optical flow algorithms—via minimizing (2) and (4) for a range of regularization schemes. In this work, we cast these evolution models into a generalized framework for reconstructing flow fields that can be locally represented by a single potential or stream function, and the flow reconstruction

results are valid in the domain where the assumption of a single potential or stream is valid. In Sec. II, we introduce the stream/potential function approach to optical flow and describe its advantages, specifically in terms of its regularization. Section III presents reconstructions of synthetic flows using the optical flow algorithms derived from Eqs. (2) and (4), as well as the flows computed within the stream/potential framework and an associated error analysis; the same is done in Sec. IV for two examples of oceanic flows.

II. A STREAM/POTENTIAL FUNCTION FRAMEWORK FOR OPTICAL FLOW

The vector fields governing many kinds of fluid flows are “potential flows,” i.e., the flow field is locally the gradient of a potential function. The potential function is denoted by ψ , and the formulations of the system evolutions corresponding to Eqs. (1) and (3) in this framework are

$$I_t = -\nabla I \cdot \nabla \psi, \quad \text{and} \quad (6)$$

$$I_t = -\text{div}(I\nabla\psi). \quad (7)$$

Define the operator A by

$$A\psi = (\nabla I + I\nabla) \cdot \nabla \psi, \quad (8)$$

then the optical flow energies (2) and (4) can be reformulated as

$$E_\alpha(\psi) = \int_{\Omega} (I_t + \nabla I \cdot \nabla \psi)^2 d\Omega + \alpha R(\psi), \quad \text{and} \quad (9)$$

$$E_\alpha(\psi) = \int_{\Omega} (I_t + A\psi)^2 d\Omega + \alpha R(\psi), \quad (10)$$

respectively, where $R(\psi)$ is an appropriate regularization of the potential function. Note that Eq. (10) reduces to Eq. (9) in the case that $I(\nabla \cdot \nabla \psi) = 0$, but the gradient of Eq. (10) does not reduce to the gradient of Eq. (9) (which is important for computing minimizers of the energies).

There are several advantages to this formulation. The first primary advantage is that any flow field reconstructed this way will necessarily be a potential flow, a scientific prior not imposed when reconstructing the components of the flow individually. The second advantage is that it allows to regularize the potential function directly.

In order to minimize Eq. (10) using a gradient-based algorithm, we must compute the gradient of $E_\alpha(\psi)$ with respect to ψ . A direct calculation gives that the gradient and Hessian of E_0 are

$$\nabla E_0 = 2A^*(I_t + A\psi) \quad \text{and} \quad \nabla^2 E_0 = 2A^*A, \quad (11)$$

where A^* is the operator adjoint of A . In particular, since the Hessian of E_0 is positive semi-definite, E_0 is a convex functional.

For flows that are locally incompressible, rather than representing the flow as the gradient of a potential function, they can instead be represented as the symplectic gradient, $\nabla_H \psi = \langle -\psi_y, \psi_x \rangle$, of a stream function. In this case, the

operator A is replaced by the operator A' defined by $A'\psi = (\nabla I + I\nabla) \cdot \nabla_H \psi$, and the optical flow energies are given by

$$E_\alpha(\psi) = \int_{\Omega} (I_t + \nabla I \cdot \nabla_H \psi)^2 d\Omega + \alpha R(\psi), \quad \text{and} \quad (12)$$

$$E_\alpha(\psi) = \int_{\Omega} (I_t + A'\psi)^2 d\Omega + \alpha R(\psi). \quad (13)$$

The potential and stream formulations lead to the same computational approaches, so the remaining analysis is performed only for the potential function formulation. Examples for each formulation are given in Sec. III.

A. Regularization of the potential function

There are two primary reasons to regularize any variational optimization problem. The first reason is to ensure that the resulting optimization problem is well-posed, which is to say that the solution to the regularized problem exists, is unique, and is stable with respect to perturbations in the input data. Moreover, it is desirable that the regularized solution closely approximates a minimizer to the unregularized energy, when the regularization parameter is small. In practice, even regularized optical flow problems are often not well-posed, as uniqueness of minimizers is rarely achievable, due to the way the data fidelity depends on the input data.

The second primary reason to regularize a variational optimization problem is to impose scientific priors on the computed solution. Given that even regularized optical flow computations are generally not well-posed, this is the fundamental purpose for regularizing optical flow. Neither of the energies (2) nor (4) allows to impose scientific priors on the flow itself, as they both regularize the components, rather than the flow as a whole. The same is true of the Helmholtz decomposition given in Ref. 24, where the regularization is imposed jointly on the div-free and curl-free components of the flow. There is some justification for regularizing the components, as images are 2D projections of the flow that will generally not exactly obey the same physics as the flows themselves. Nonetheless, it is desirable to be able to enforce that the computed flow is constructed using the same physical principles that are assumed on the flow itself.

It is clear that imposing scientific priors on the flow is not equivalent to imposing the same prior on the components of the flow, but the problem is more subtle than that. Suppose it is known that a given flow is sparse. Sparse reconstruction is often performed using L^1 regularization,²⁵ which in the case of Eq. (2) or Eq. (4) would imply that

$$R(u, v) = \int_{\Omega} |u| + |v| d\Omega. \quad (14)$$

With this regularization, however, the Euler-Lagrange equations for u and v couple u and v only in the terms corresponding to the data fidelity and not in the terms corresponding to the regularization. In this sense, the regularizations of u and v occur independently. Thus, the solution will favor a sparse

u and a sparse v , but this does not imply that the flow field will be sparse since the complements of the supports of u and v need not largely overlap. This is just to say that u could be 0 in many places and v could be 0 in many places, but they need not be 0 in the same places. Within the potential function formulation of optical flow, imposing sparsity on the computed flow field is quite natural. The regularization that will accomplish this is the total variation of the potential function,

$$R(\psi) = \int_{\Omega} |\nabla \psi| d\Omega. \quad (15)$$

(Note that the total variations of $\nabla \psi$ and $\nabla_H \psi$ are equal, so the same result holds for the stream formulation.) The potential function formulation allows to impose the sparsity directly on the flow, which does not occur when reconstructing u and v separately.

Since optical flow computations are rarely well-posed, the fundamental point here is that choosing regularization schemes for optical flow does not follow the classical, mathematical guidelines found in the inverse problems literature. Instead, regularizing optical flow should be viewed as a part of the modeling of the flow. For example, in Ref. 26, a regularization scheme is derived that is the most general regularization not penalizing rigid body motion, making it a natural regularization scheme for flows that are combinations of pure rotations, translations, etc. Mathematically, it means that the computation of the flow takes place in a highly restricted space of affine mappings, but it is more important to analyze the properties of such functions than it is to define and analyze the space rigorously.

For the data fidelity in Eq. (2), adapting the regularization has been explored in some detail by Weickert *et al.* in Ref. 27. Their analysis primarily describes the framework in which one can implement different regularizations, and they give several examples. The effect of different regularization schemes for optical flow in a fluid dynamics setting is addressed in Refs. 12 and 13, though the authors there use a different data fidelity term.

Table I shows 6 regularization terms for potential-based optical flow. The simplest regularization term, R_1 —which is actually a step backward from the Horn-Schunck method—is to use the $H^2(\Omega)$ norm of the potential function. This regularization has the advantage that it is coercive and strictly convex, which ensures the uniqueness in $H^2(\Omega)$ of minimizers to the optical flow functional, which, as noted above, is not of primary importance for optical flow. The second regularizer, R_2 , is the Horn-Schunck regularization. The regularization R_4 comes from the “engineering strain tensor” formulation of optical flow, a full description and explanation of which can be found in Ref. 26. Finally, R_5 is the potential and stream function form of the first-order “div-curl” regularization proposed by Suter.²³

The gradient of each of the above regularizations results in a linear contribution to the Euler-Lagrange equation, as do the fidelity terms. Thus, a first-order necessary condition that ψ^* be a minimizer of Eq. (10) regularized with R_2 is that it be a solution to the linear PDE

TABLE I. Six potential (stream) function regularization schemes with descriptions.

| | Regularization term | Purpose of regularization |
|-------|---|--|
| R_1 | $\int_{\Omega} \psi^2 + \psi_x^2 + \psi_y^2 + \psi_{xx}^2 + \psi_{yy}^2 d\Omega$ | Ensures uniqueness of minimizers in $H^2(\Omega)$ |
| R_2 | $\int_{\Omega} \psi_{xx}^2 + \psi_{xy}^2 + \psi_{yx}^2 + \psi_{yy}^2 d\Omega$ | Horn-Schunck regularization |
| R_3 | $\int_{\Omega} \psi_x^2 + \psi_y^2 d\Omega$ | Corresponds to regularization of u and v via the $L^2(\Omega)$ norm |
| R_4 | $\int_{\Omega} (\psi_{xx} - \psi_{yy})^2 + (\psi_{xy} + \psi_{yx})^2 d\Omega + \int_{\Omega} \psi_{yxx}^2 + \psi_{xyy}^2 d\Omega$ | Strain tensor regularization, does not penalize rigid motion ²⁶ |
| R_5 | $\int_{\Omega} (\psi_{xx} + \psi_{yy})^2 + (\psi_{xy} - \psi_{yx})^2 d\Omega$ | Provides smoothness and does not penalize hyperbolic flow (div-curl reg. ²³) |
| R_6 | $\int_{\Omega} (\psi_{xx} - \psi_{yy})^2 + (\psi_{yx} - \psi_{xy})^2 d\Omega$ | Provides smoothness and does not penalize rotational flow |

$$[2A^*A + \alpha(B + B^*)]\psi = -2A^*I_t, \quad (16)$$

where A is given by Eq. (8) and $B = D_{xx}^*D_{xx} + D_{yx}^*D_{yx} + D_{xy}^*D_{xy} + D_{yy}^*D_{yy}$. Here, D_{xx} is the second derivative operator, and D_{xx}^* its operator adjoint. In practice, the derivatives are computed using finite differences in a matrix form, and the adjoint operator reduces to a matrix transpose. Equation (16) can be solved using iterative techniques or direct methods for solving sparse linear systems. In practice, we use a direct LU factorization for solving all linear Euler-Lagrange equations. Note that when the regularization results in a linear contribution to the Euler-Lagrange equation, the matrix B is self-adjoint, and Eq. (16) simplifies to $(A^*A + \alpha B)\psi = -A^*I_t$, in which case a Cholesky factorization is also possible. This simplification is not the case in general for regularizations contributing nonlinearly to the Euler-Lagrange equation. See Ref. 28 for an analysis of total variation regularization for optical flow in the potential and u - v formulations of optical flow.

Regularizations R_2 and R_3 will be used to demonstrate the potential and stream function approaches to computing optical flow in Sec. III; all 6 regularizations are compared in Sec. III B for both formulations (9) and (10); and in Sec. III A we address the selection of the regularization parameter.

III. SYNTHETIC FLOWS

In this section, we demonstrate the performance of potential and stream function-based optical flow for capturing several different kinds of flows. For our initial experiments, we begin with a potential or stream function, evolve an initial density, and reconstruct the function from two time instances of the density evolution. The first example is a flow with potential function

$$\psi(x, y) = \sin(x)\cos(y). \quad (17)$$

We integrate the initial density shown in Fig. 1(a) forward in time under the evolution model (3) to the density shown in Fig. 1(b), under the flow field

$$\nabla\psi(x, y) = \langle u, v \rangle = \langle \cos(x)\cos(y), -\sin(x)\sin(y) \rangle. \quad (18)$$

By construction, this is a potential flow, but it is not a stream flow, as it corresponds to a source in the flow, which is compressible.

Fig. 1(c) shows the true flow by which image (a) was evolved to (b), and Fig. 2 shows computed reconstructions

for the potential function formulation and the u - v formulation. The reconstructions computed within each formulation are shown for both the continuity equation (first row) and conservation of intensity (second row) evolution models and regularizations R_2 (first and third columns) and R_3 (second and fourth columns). For this flow both the potential function approach and the u - v approach produce correct flow fields with both evolution models and both regularizations. Both formulations show larger errors around the boundary of the image with R_3 and the continuity equation evolution model. A detailed error analysis is given in Sec. III B.

Another flow structure to be reconstructed is that about a hyperbolic fixed point, so the next example is to compute the flow determined by the stream function

$$\psi(x, y) = x^2 - y^2, \quad (19)$$

on \mathbb{R}^2 . The true flow is shown in Fig. 3(c) on the window $[-0.5, 0.5] \times [-0.5, 0.5]$, and the two time instances between which the flow is computed are shown in images (a) and (b).

In this case, the conservation of intensity (6) and continuity equation (7) models result in the same density evolution, since $\nabla \cdot \nabla_H \psi = 0$. (Note also that, when integrating this density forward in time, the stream function and u - v formulations result in the same evolution, so it is appropriate to

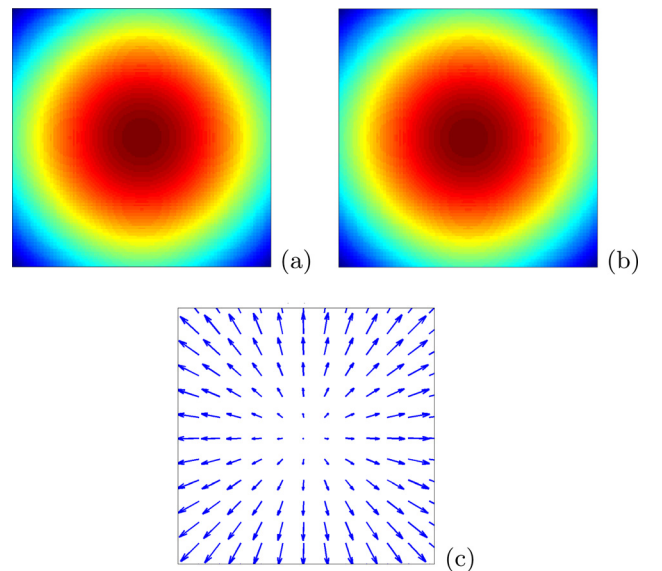


FIG. 1. Diffusive Flow—Images (a) and (b) show the initial and final time instances of the density evolution according to (7) with potential function given by Eq. (18). The true flow field is shown in (c).

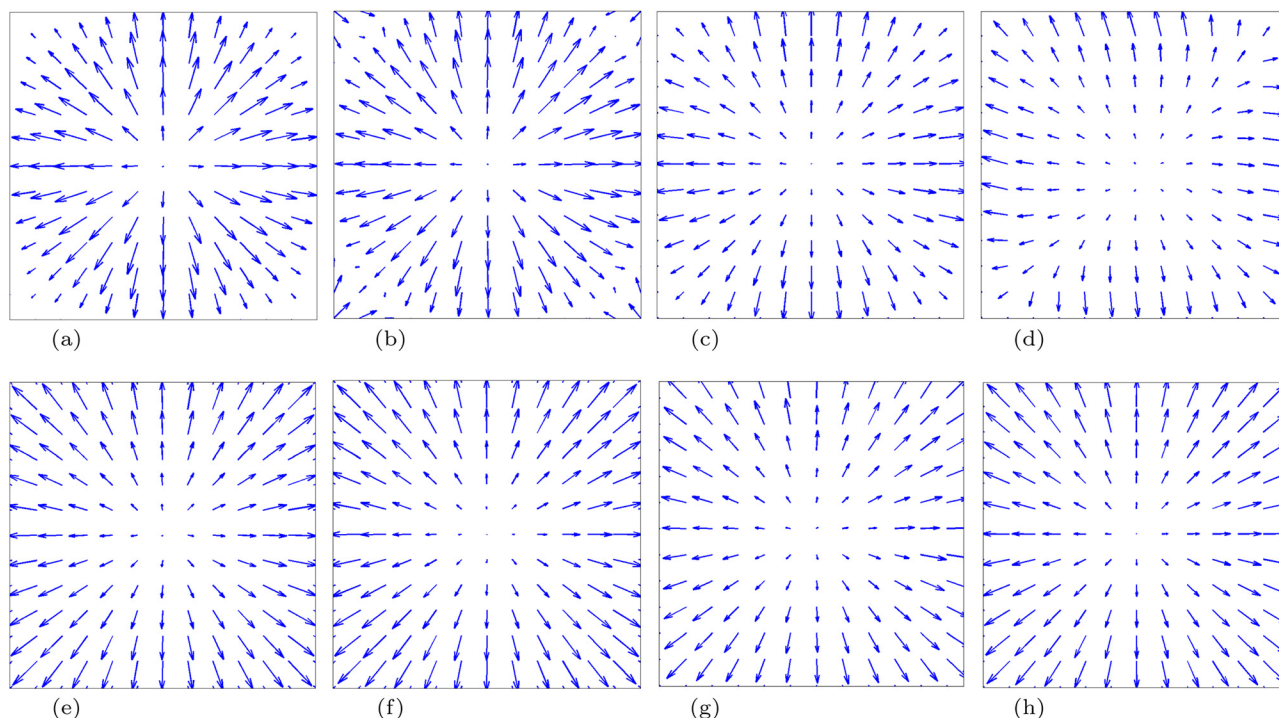


FIG. 2. Diffusive Flow—Reconstructed flow fields using R_2 and R_3 and evolution models (6) and (7) within the ψ and u - v optical flow frameworks. Both frameworks result in reasonable reconstructions with both evolution models and both regularizations, though both ψ and u - v approaches show errors around the boundary for R_3 in model (7) (images (b) and (d)). Mean angular errors are given in Table II.

compare the reconstruction techniques on data generated from either approach.) Nonetheless, the reconstructed flow fields given by the two different models are not the same, as the gradients of the corresponding optical flow functionals do not coincide. Fig. 4 shows the reconstructions of the flow between Figs. 3(a) and 3(b).

In the case of either regularization and either evolution model, the stream function approach gives a reasonable reconstruction. The u - v method gives a reasonable reconstruction for either evolution model when regularized with

R_2 but does not give a reasonable reconstruction with either evolution model when regularized with R_3 . This is due to the fact that the pair $\langle u, v \rangle$ that minimizes Eq. (4) or Eq. (2) when regularized with R_3 is not a stream flow. That is to say that the u - v approach with regularization R_3 fails to enforce the model of a stream flow.

Our third physical structure we wish to reconstruct is that of a vortex—or gyre—so we integrate forward an initial density according to Eq. (7) with

$$\psi(x, y) = \sin(\pi x)\sin(\pi y), \quad (20)$$

on \mathbb{R}^2 , where we visualize just the subset $[0, 1] \times [0, 1]$. This represents the flow about an elliptic fixed point. As above, the two models (6) and (7) result in the same density evolution. The true flow is shown in Fig. 5(c), and the two time instances between which the flow is computed are shown in images (a) and (b).

As can be seen in Fig. 6, this example tells a similar story to the previous. The stream function reconstruction methods reconstruct the gyre flow, regardless of the evolution model or regularization, whereas the u - v approach is only capable of producing a reasonable reconstruction with the conservation of intensity model and R_2 .

A. Regularization parameter selection

The selection of the regularization parameter for optical flow techniques has not been widely addressed in the optical flow literature, and there are important issues that should be noted. The value of the regularization parameter is important in nearly all applications, and for optical flow that is especially true. In order to choose the appropriate value of the

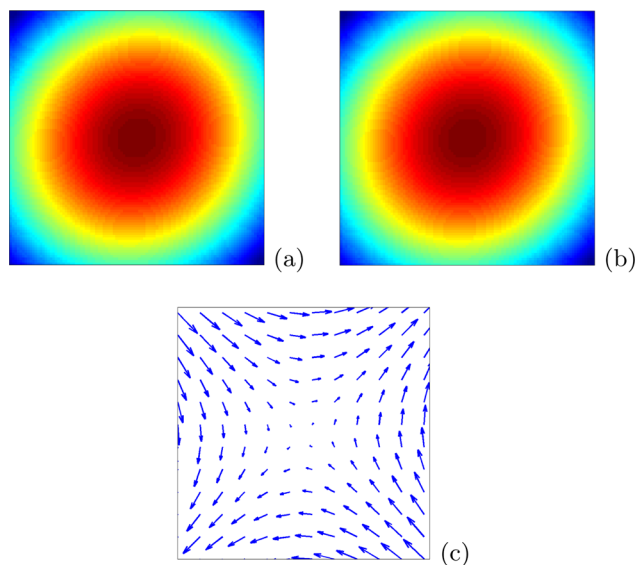


FIG. 3. Hyperbolic Flow—Images (a) and (b) show the initial and final time instances of the density evolution according to Eq. (7) with potential function given by Eq. (19). The true flow field is shown in (c).

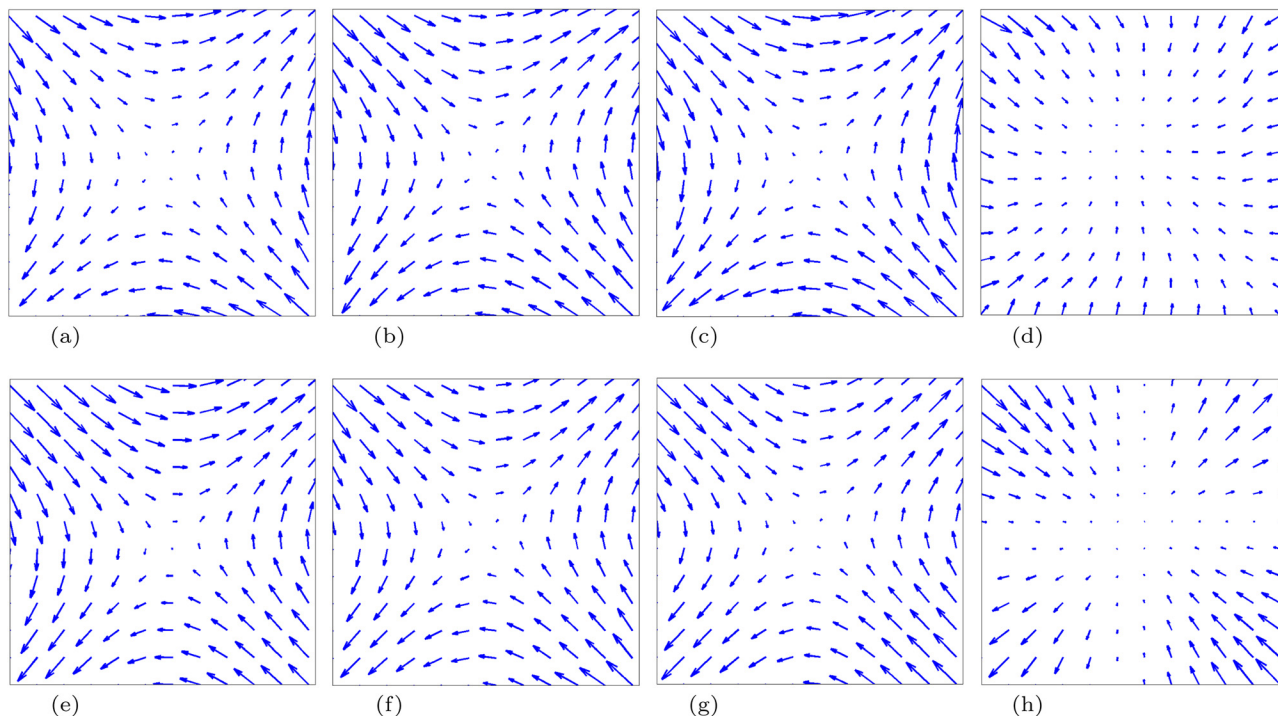


FIG. 4. Hyperbolic Flow—Reconstructed flow fields using R_2 and R_3 and evolution models (6) and (7) within the ψ and $u-v$ optical flow frameworks. The stream function method successfully reconstructs the flow for both regularizations and both evolution models, whereas the $u-v$ approach cannot successfully reconstruct with regularization R_3 in either evolution model. Mean angular errors are given in Table II.

regularization parameter α , it is possible to use a classical method such as the L -curve,^{29,30} U -curve,^{31,32} or generalized cross-validation (GCV), and its generalizations.^{33,34} It is well-known that each of these methods—despite being ubiquitous in the literature—have limitations (for example, Refs. 35 and 36). Fig. 7 shows the mean angular error (MAE, see Sec. III B) vs. regularization parameter curves for the gyre flow, reconstructed using the stream function approach with regularizations R_4 (on the top) and R_2 (on the bottom). For regularization R_4 , the U -curve method selects a

regularization parameter that is very close to the minimum mean angular error, but the other two methods select parameters whose corresponding MAE is almost twice the minimum. The success of the U -curve in the first case is not a general result, and none of these three methods for regularization parameter selection performs well with regularization R_2 . This suggests that the development of regularization parameter selection algorithms specific to optical flow is important future work.

For each reconstruction in this work, we have performed an exhaustive search to find a regularization parameter that approximately minimizes the MAE (described further in Sec. III B). Each of the images presented in figures above shows the best reconstruction that can be achieved with these formulations, with respect to the regularization parameter choice.

B. Error analysis

In order to quantitatively demonstrate the improvement of the stream function approach, we compute the modified mean angular error³⁷ for each of the 3 flows of the previous section with each of the 6 regularization schemes in Table I, as well as several combinations of regularizations that ensure uniqueness of the flow.

Table II shows the mean angular error for the potential (top half of table) and $u-v$ formulations (bottom half of table) of optical flow with both the continuity equation-based and conservation of intensity-based evolution models and all 6 regularization schemes described in Table I. For the hyperbolic flow, the potential function formulation results in a smaller mean angular error than the $u-v$ formulation for both evolution models and all regularization schemes. The best reconstruction is computed by the potential function approach

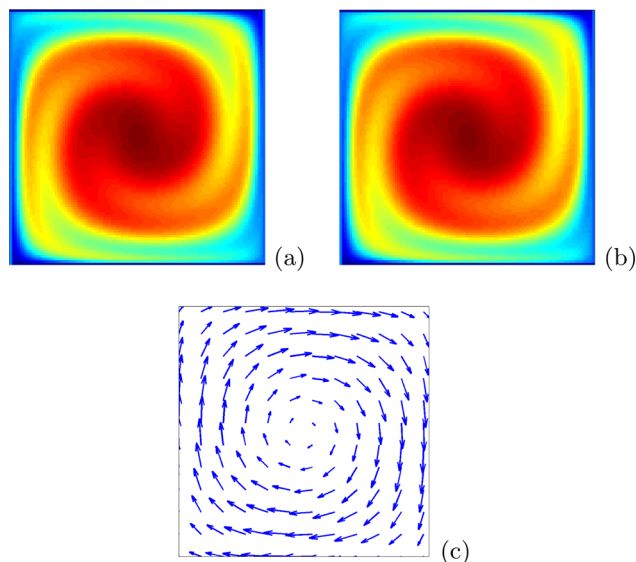


FIG. 5. Gyre Flow—Images (a) and (b) show two later time instances of an initial density that has been evolved according to Eq. (7) with stream function given by Eq. (20). The true flow field is shown in (c).

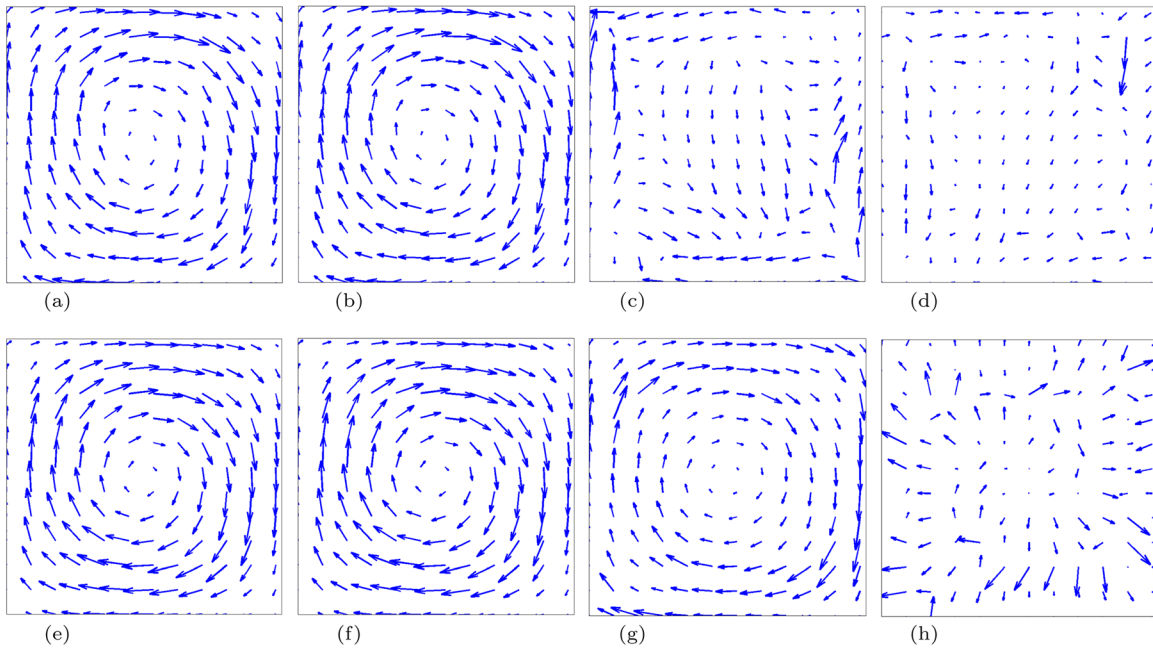


FIG. 6. Gyre Flow—Reconstructed flow fields using R_2 and R_3 and evolution models (6) and (7) within the ψ and $u-v$ optical flow frameworks. In this case, the $u-v$ approach can only reconstruct the vortex with the conservation of intensity evolution model and R_2 , whereas the stream function method reconstructs the gyre with either model or regularization. Mean angular errors are given in Table II.

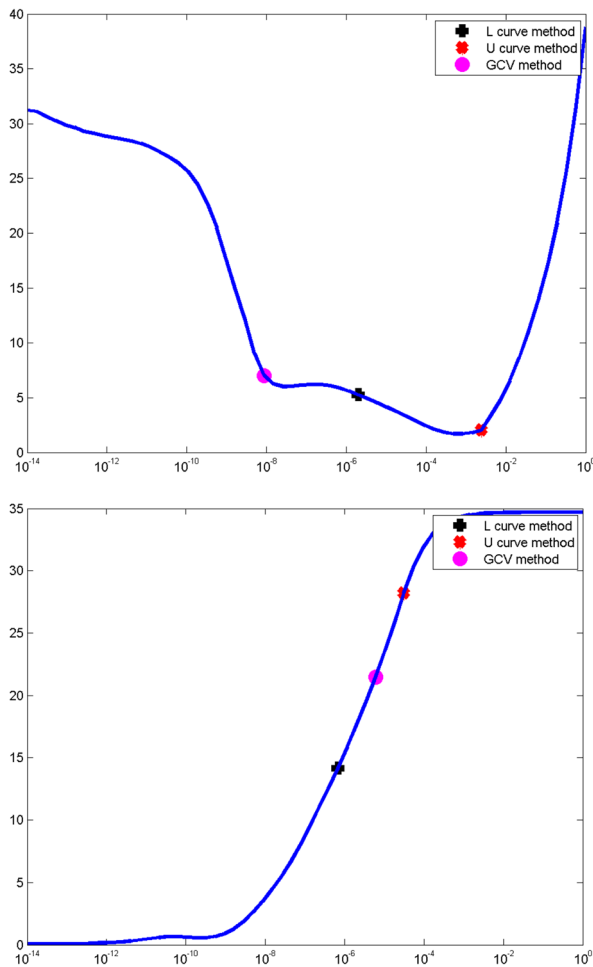


FIG. 7. Regularization Parameter Selection—The two plots show examples of the mean angular error versus regularization parameter, for the gyre flow reconstruction within the stream function framework for regularizations R_4 (left) and R_2 (right). In each case, the regularization parameters selected by the L -curve, U -curve, and Generalized Cross Validations methods are shown.

with the conservation of intensity data fidelity and R_3 , with a mean angular error of 0.057° .

The gyre flow is better reconstructed using the stream function formulation with the continuity equation and all regularizations, as the $u-v$ approach fails to accurately reconstruct the gyre using the continuity equation with any regularization. With the conservation of intensity evolution model, the $u-v$ approach does reconstruct the gyre well with all regularizations except R_3 . The best reconstruction is computed with the stream function approach, conservation of intensity, and R_2 , with a mean angular error of 1.1° .

With the conservation of intensity data fidelity, the ψ approach well reconstructs the diffusive flow with all regularizations, but the $u-v$ approach gives lower mean angular errors for all regularizations with conservation of intensity and with R_4 , R_5 , and R_6 with the continuity equation. The best reconstruction is computed with $u-v$, conservation of intensity, and $R_2 + R_3$, with a mean angular error of 0.647° , though the potential function formulation with conservation of intensity and $R_2 + R_3$ results in an MAE of only 0.782° .

The potential function formulation captures two of the dynamical structures we wish to compute using optical techniques better than the classical $u-v$ formulation, elliptic fixed points (like the gyre flow) and hyperbolic fixed points (like in the hyperbolic flow). The $u-v$ formulation results in a lower mean angular error relative to the potential function formulation around a source (like the diffusive flow), but the potential function framework still does a good job of capturing the structure.

IV. APPLICATIONS AND EXAMPLES

We now highlight our method with examples from oceanographic data sets.

TABLE II. Mean angular error of flow field reconstructions for hyperbolic (Fig. 4), gyre (Fig. 6), and diffusive (Fig. 2) flows within the potential function formulation (top half of the table) and within the u - v formulation (bottom half of the table). For each data set, the MAE is computed for the Continuity Equation (CE) (7) and the Conservation of Intensity (CI) (6) evolution models. The errors are given for each of the 6 regularization schemes described in Table I, as well as two schemes that ensure uniqueness of minimizers for the potential function approach, $R_1 + R_2$ and $R_1 + R_3$, and one scheme that ensure uniqueness for the u - v approach, $R_2 + R_3$. There is no u - v formulation for R_1 .

| Flow field potential, ψ | Evolution model | R_1 | R_2 | R_3 | R_4 | R_5 | R_6 | $R_1 + R_2$ | $R_1 + R_3$ |
|------------------------------|-----------------|---------|---------|---------|---------|---------|---------|-------------|-------------|
| Hyperbolic | Cont. Eq. | 0.096° | 0.091° | 0.082° | 0.093° | 0.100° | 0.093° | 0.091° | 0.088° |
| Hyperbolic | Cons. Int. | 0.062° | 0.062° | 0.057° | 0.062° | 0.062° | 0.062° | 0.062° | 0.057° |
| Gyre | Cont. Eq. | 30.824° | 3.195° | 9.813° | 10.206° | 9.843° | 10.751° | 3.897° | 32.064° |
| Gyre | Cons. Int. | 20.749° | 1.100° | 1.637° | 1.746° | 1.713° | 1.721° | 1.100° | 21.863° |
| Diffusive | Cont. Eq. | 8.622° | 1.616° | 11.560° | 4.110° | 4.028° | 6.002° | 1.616° | 8.622° |
| Diffusive | Cons. Int. | 2.755° | 2.756° | 1.275° | 2.170° | 2.144° | 2.170° | 2.169° | 0.782° |
| Flow field $u-v$ | Evolution model | R_1 | R_2 | R_3 | R_4 | R_5 | R_6 | $R_1 + R_3$ | $R_2 + R_3$ |
| Hyperbolic | Cont. Eq. | * | 1.706° | 47.094° | 2.084° | 1.400° | 2.292° | * | 1.706° |
| Hyperbolic | Cons. Int. | * | 1.141° | 27.383° | 1.509° | 1.509° | 1.576° | * | 0.602° |
| Gyre | Cont. Eq. | * | 42.680° | 40.991° | 43.133° | 41.975° | 36.376° | * | 40.560° |
| Gyre | Cons. Int. | * | 2.624° | 48.573° | 2.610° | 2.618° | 2.661° | * | 2.489° |
| Diffusive | Cont. Eq. | * | 2.710° | 8.678° | 2.782° | 2.666° | 0.957° | * | 2.700° |
| Diffusive | Cons. Int. | * | 0.647° | 1.104° | 0.895° | 0.895° | 1.228° | * | 0.647° |

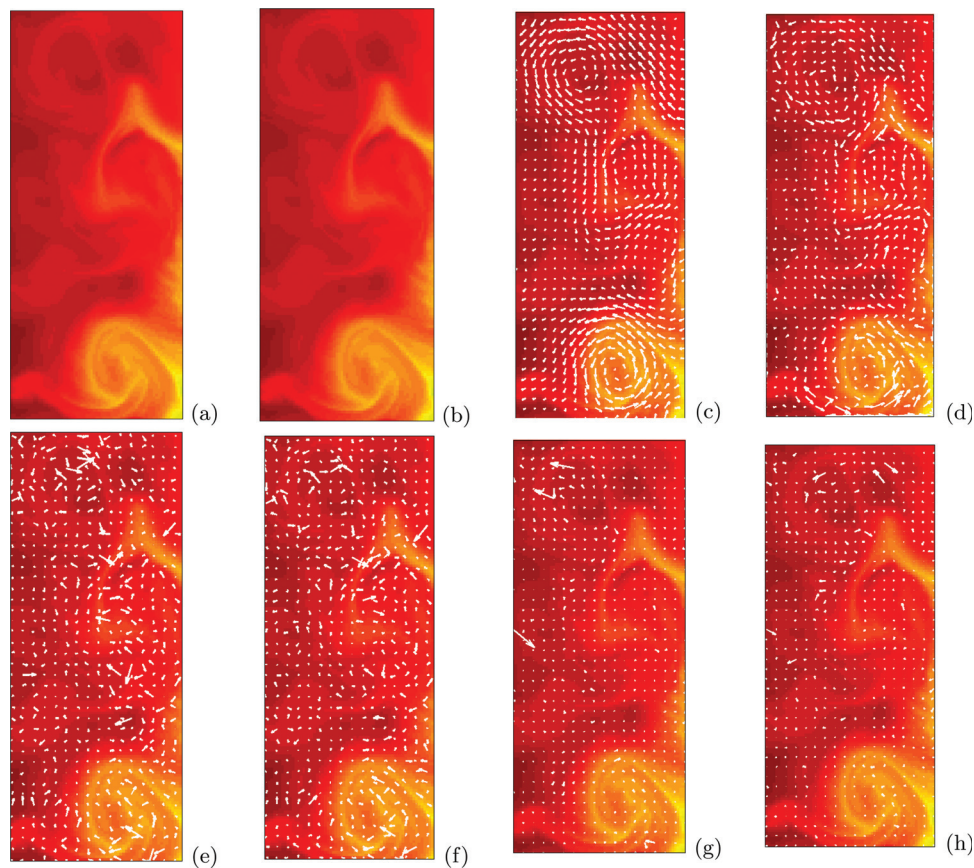


FIG. 8. Sea Surface Temperature Flow—Images (a) and (b) show two sea surface temperature along the coast of Oregon (USA) from two different days in August 2002. Images (c) and (d) show the optical flow field, computed using the stream function method with R_2 and R_3 regularizations, images (e) and (f) show the optical flow field, computed using the potential function method with R_2 and R_3 regularizations, and images (g) and (h) show the optical flow field using the traditional u - v approach with R_2 and R_3 . In all cases, the reconstruction is computed using the conservation of intensity evolution model. Note that the stream function approach captures the vortical structures in the flow, which are not captured by either the potential or u - v methods.

A. An example using sea surface data

To illustrate the method, we consider an image sequence generated from a Regional Ocean Model System (ROMS) along the Oregon Coast.³⁸ Oceanic flows are three-dimensional but are dominated by Coriolis force, balanced by pressure gradients, or so-called geostrophic balance. The geostrophic balance condition is often used to create 2D flow equations to understand and model features of ocean surface dynamics. The most well developed theories go under the monikers of geostrophic turbulence and surface quasi-geostrophic turbulence.³⁹ Both theories are transport equations of a scalar quantity by a non-divergent flow, which conserve an infinity of invariants. That is, the quasi-geostrophic equations have a Hamiltonian structure.^{40,41} Alternatively, we can also introduce constraints that we expect to hold only for limited areas of the surface flow, like eddies.⁴² Here, we simply show an illustrative example of how such prior information can be easily added to an optical flow model.

Fig. 8 shows two time instances of sea surface temperature off the coast of Oregon, U.S.A. (images (a) and (b)). The

data are generated from an 3D ocean model along the Oregon shelf that includes wind-driven and tidal flows, and is informed by satellite data.³⁸ The model covers 540 by 300 km (between approximately 41 to 46 N, and -125 to -124 W) with an hourly temporal resolution, and 1 km horizontal resolution. The model is verified against both buoy data and satellite data, in particular sea surface temperature (SST) data from the Geostationary Operational Environmental Satellite (GOES). The coastal SST data used here is taken from hourly simulation results from the first week of August, 2002.

Two time instances of the flow are shown in Fig. 8, as are the computed optical flow fields using the potential, stream and u - v formulations of the continuity equation-based optical flow with regularization R_2 . In general, it would not be known ahead of time if the flow is better computed assuming incompressibility or not, so it makes sense to compare not just the potential function method vs. the u - v method but also the potential function vs. stream function formulations.

The stream function formulation correctly reconstructs the vortices in the flow, whereas neither the potential nor the

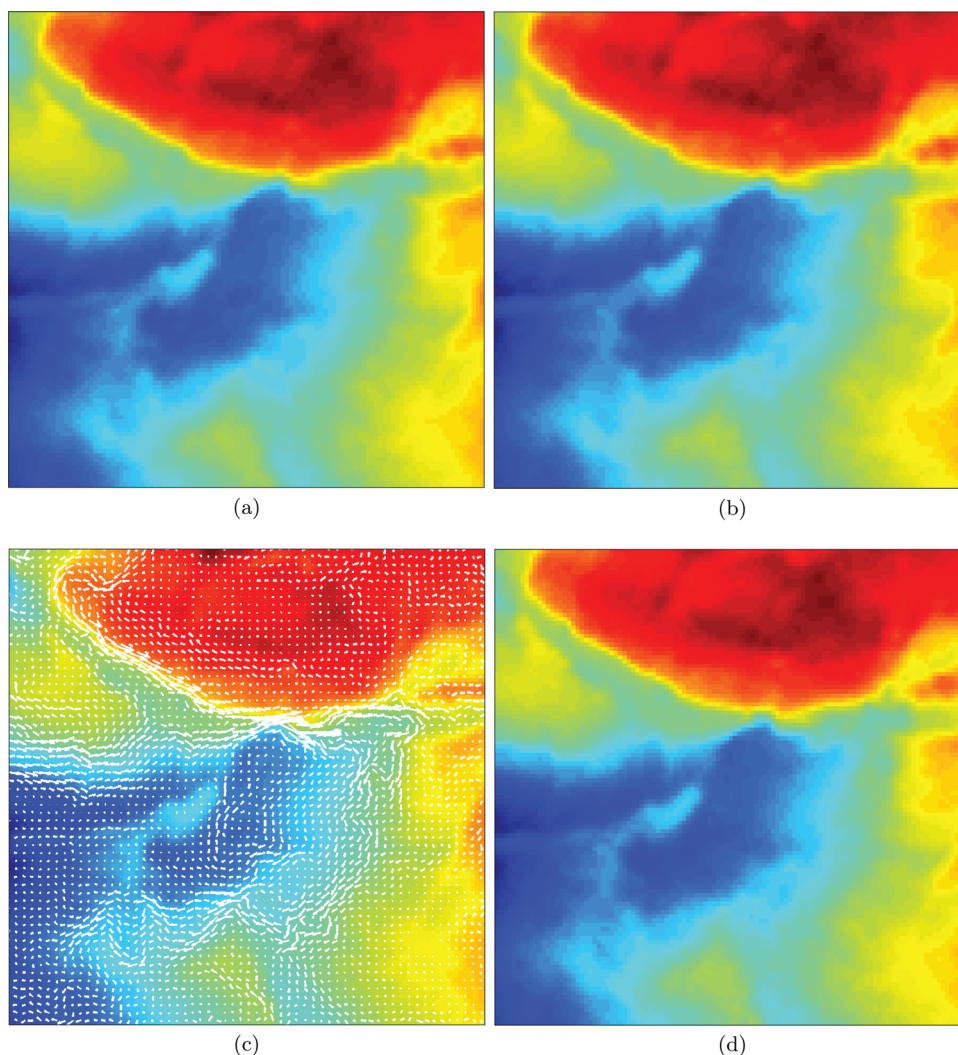


FIG. 9. GOCI Flow—Images (a) and (b) show products movements in the seas of South Korea. Image (c) shows the optical flow field, computed using the stream function method with R_2 regularization. Image (d) shows the reconstructed second image by evolving first image forward in time under the evolution model (3) with the computed flow field as shown in image (c). The mean relative error is 2.21% per grid point, whereas the mean relative error using the u - v formulation is 5.32%.

u - v method is capable of doing so. In order to analyze the dynamics of the flow, it is thus best to assume the incompressibility of the flow and to compute the vector field using the stream function formulation. This vector field can then be used to determine things like mass transport and coherent sets. Beginning directly from the image data allows to determine the flow dynamics without the use of the model.⁴³

B. Example from GOCI satellite

To verify the accuracy of the stream function method, we apply our method to a new data set which represents product movements in the seas of South Korea. The data are obtained from a geosynchronous satellite from South Korea called "GOCI." The images (a) and (b) in Fig. 9 are 10 min apart from each other. In this case, we compute the vector field using these two images as shown in image (c) in Fig. 9. In the absence of a known vector field, a study of image evolution can serve to validate the method. Now, we integrate the first image shown in Fig. 9(a) forward in time under the evolution model (3) with the computed flow field shown in Fig. 9(c) to reconstruct the second image. The reconstructed second image is shown in Fig. 9(d).

To compare the actual image and the reconstructed image, the relative error was computed over the image domain and then averaged the magnitude of the error over the domain to obtain mean relative error. The mean relative error for the stream function approach is 2.21% and the u - v approach is 5.32%.

V. CONCLUSIONS

We have presented an alternative formulation to the optical flow problem. Rather than reconstructing the components of the flow governing an image intensity evolution, we directly reconstruct the flow potential. By regularizing the potential function, we are able to impose scientific priors directly on the flow, rather than on the components of the flow, thus respecting the underlying physics governing the fluid flow.

ACKNOWLEDGMENTS

The authors thank John Osborne and Alex Kurapov for providing access to data from their Regional Ocean Modeling System (ROMS) during the summer of 2002. Aaron Luttman, Erik M. Bollt, Ranil Basnayake, and Sean Kramer work was supported by the U.S. Office of Naval Research under Grant No. N00014-09-1-0647.

¹B. K. P. Horn and B. G. Schunck, "Determining optical flow," *Artif. Intell.* **17**, 185–203 (1981).

²W. Bresky and J. Daniels, "The feasibility of an optical flow algorithm for estimating atmospheric motion," in *Proceedings of the Eighth Int. Winds Workshop, Beijing, China* (2006), pp. 24–28.

³T. Brox and J. Malik, "Large displacement optical flow: Descriptor matching in variational motion estimation," *IEEE Trans. Pattern Anal. Mach. Intell.* **33**, 500–513 (2011).

⁴A. Bruhn, J. Weickert, C. Feddern, T. Kohlberger, and C. Schnorr, "Real-time optical flow computation with variational methods," in *CAIP 2003* (Springer, 2003), pp. 222–229.

⁵S. Gupta, E. N. Gupta, and J. L. Prince, "On div-curl regularization for motion estimation in 3-d volumetric imaging," in *In Proc. International Conf. on Image Proc. (ICIP96)* (1996), pp. 929–932.

⁶H. W. Haussecker and D. J. Fleet, "Computing optical flow with physical models of brightness variation," *IEEE Trans. Pattern Anal. Mach. Intell.* **23**, 661–673 (2002).

⁷Y. H. Kim, A. M. Martínez, and A. C. Kak, "A local approach for robust optical flow estimation under varying illumination," in *Proc. British Machine Vision Conf* (2004).

⁸J. Marzat, Y. Dumortier, and A. Ducrot, "Real-time dense and accurate parallel optical flow using cuda," in *Symposium on Advances in Image and Video Technology* (2009).

⁹M. Werlberger, W. Trobin, T. Pock, A. Wedel, D. Cremers, and H. Bischof, "Anisotropic Huber- L^1 optical flow," in *Proceedings of the British Machine Vision Conference* (2009).

¹⁰G. M. Quénot, J. Pakleza, and T. A. Kowalewski, "Particle image velocimetry with optical flow," *Exp. Fluids* **25**, 177–189 (1998).

¹¹T. Corpetti, D. Heitz, G. Arroyo, E. Mémin, and A. Santa-Cruz, "Fluid experimental flow estimation based on an optical-flow scheme," *Exp. Fluids* **40**, 80–97 (2006).

¹²D. Auroux, "Extraction of velocity fields for geophysical fluids from a sequence of images," in *Acoustics, Speech, and Signal Processing, IEEE Proceedings on (ICASSP)* (2009), pp. 961–964.

¹³D. Auroux and J. Fehrenbach, "Identification of velocity fields for geophysical fluids from a sequence of images," *Exp. Fluids* **50**, 313–328 (2011).

¹⁴C. Cassisa, V. Prinet, L. Shao, S. Simoens, and C. L. Liu, "Optical flow robust estimation in a hybrid multi-resolution MRF framework," in *Acoustics, Speech and Signal Processing, 2008. ICASSP 2008. IEEE International Conference on* (2008), pp. 793–796.

¹⁵D. Heitz, E. Mémin, and C. Schnorr, "Variational fluid flow measurements from image sequences: Synopsis and perspectives," *Exp. Fluids* **48**, 369–393 (2010).

¹⁶A. Luttman, E. Bollt, and J. Holloway, "An optical flow approach to analyzing species density dynamics and transport," *J. Comput. Math.* **30**, 249–261 (2012).

¹⁷A. Luttman, E. Bollt, R. Basnayake, and S. Kramer, "A stream function approach to optical flow with applications to fluid transport dynamics," in *Proc. Appl. Math. Mechanic* (2011), Vol. 11, pp. 855–856.

¹⁸T. Corpetti, E. Mémin, and P. Pérez, "Adaptation of standard optic flow methods to fluid motion," in *9th Int. Symp. Flow Visualisation* (2000) pp. 1–10.

¹⁹T. Corpetti, E. Mémin, and P. Pérez, "Estimating fluid optical flow," in *ICPR* (2000) pp. 7045–7048.

²⁰T. Corpetti, E. Mémin, and P. Pérez, "Dense estimation of fluid flows," *IEEE Trans. Pattern Anal. Mach. Intell.* **24**, 365–380 (2002).

²¹T. Corpetti, E. Mémin, and P. Pérez, "Dense motion analysis in fluid imagery," in *Proc. 7th Eur. Conf. Computer Vision*, edited by A. Heyden (2002), pp. 676–691.

²²E. Mémin and T. Corpetti, "Dense fluid flow estimation," Tech. Rep. (INRIA, 2000).

²³D. Suter, "Motion estimation and vector splines," in *Proc. Conf. Comp. Vision Pattern Rec* (IEEE, 1994), pp. 939–942.

²⁴T. Kohlberger, E. Mémin, and C. Schnorr, "Variational dense motion estimation using the helmholtz decomposition," in *Scale Space '03*, edited by L. D. Griffin and M. Lillholm (Isle of Skye, UK, 2003), Vol. 2695, pp. 432–448.

²⁵M. Schmidt, G. Fung, and R. Rosales, "Fast optimization methods for l1 regularization: A comparative study and two new approaches," *Mach. Learn.* **4701**, 286 (2007).

²⁶D. Koppel, C.-M. Tsai, and Y.-F. Wang, "Regularizing optical-flow computation using tensor theory and complex analysis," in *Computer Vision and Pattern Recognition Workshops, 2008. CVPRW'08. IEEE Computer Society Conference on* (2008), pp. 1–6.

²⁷J. Weickert, A. Bruhn, N. Papenberg, and T. Brox, "Variational optic flow computation: From continuous models to algorithms," in *International Workshop on Computer Vision and Image Analysis, IWCVIA'03, Las Palmas de Gran Canaria*, edited by L. Alvarez (2003).

²⁸R. Basnayake, A. Luttman, and E. Bollt, "A lagged diffusivity method for computing total variation regularized fluid flow," *Contemp. Math.* **586**, 57–64 (2013).

²⁹P. C. Hansen, "Analysis of discrete ill-posed problems by means of the L-curve," *SIAM Rev.* **34**, 561–580 (1992).

³⁰P. C. Hansen, "The L-curve and its use in the numerical treatment of inverse problems," in *Computational Inverse Problems in Electrocardiology, Advances*

- in *Computational Bioengineering*, edited by P. Johnston (WIT Press, 2000) pp. 119–142.
- ³¹D. Krawczyk-Stado and M. Rudnicki, “Regularization parameter selection in discrete ill-posed problems—the use of the U-curve,” *Int. J. Appl. Math. Comput. Sci.* **17**, 157–164 (2007).
- ³²D. Krawczyk-Stado and M. Rudnicki, “The use of L-curve and U-curve in inverse electromagnetic modelling,” *Intell. Comput. Tech. Appl. Electromagn.* **119**, 73–82 (2008).
- ³³G. Golub, M. Heath, and G. Wahba, “Generalized cross-validation as a method for choosing a good ridge parameter,” *Technometrics* **21**, 215–223 (1979).
- ³⁴M. A. Lukas, “Strong robust generalized cross-validation for choosing the regularization parameter,” *Inverse Probl.* **24**, 034006 (2008).
- ³⁵C. R. Vogel, “Non-convergence of the L-curve regularization parameter selection method,” *Inverse Probl.* **12**, 535–548 (1996).
- ³⁶M. Hanke, “Limitations of the L-curve method in ill-posed problems,” *BIT* **36**, 287–301 (1996).
- ³⁷B. McCane, K. Novins, D. Crannitch, and B. Galvin, “On benchmarking optical flow,” *Comput. Vis. Image Underst.* **84**, 126–143 (2001).
- ³⁸J. J. Osborne, A. L. Kurapov, G. D. Egbert, and P. M. Kosro, “Spatial and temporal variability of the m2 internal tide generation and propagation on the oregon shelf,” *J. Phys. Oceanogr.* **41**, 2037–2062 (2011).
- ³⁹G. K. Vallis, *Atmospheric and Oceanic Fluid Dynamics* (Cambridge University Press, Cambridge, U.K., 2006) p. 745.
- ⁴⁰J. Allen and D. D. Holm, “Extended-geostrophic hamiltonian models for rotating shallow water motion,” *Physica D* **98**, 229–248 (1996).
- ⁴¹D. D. Holm and V. Zeitlin, “Hamilton’s principle for quasigeostrophic motion,” *Phys. Fluids* **10**, 800–806 (1998).
- ⁴²D. P. Marshall, J. R. Maddison, and P. S. Berloff, “A framework for parameterizing eddy potential vorticity fluxes,” *J. Phys. Oceanogr.* **42**, 539–557 (2012).
- ⁴³E. M. Bollt, A. Luttman, S. Kramer, and R. Basnayake, “Measurable dynamics analysis of transport in the Gulf of Mexico during the oil spill,” *Int. J. Bifurcation Chaos* **22**, 1230012 (2012).